This is the author accepted manuscript version of: D. V. Antonov, S. Tonini, G. E. Cossali, V. V. Dolgikh, P. A. Strizhak, S. S. Sazhin; Droplet heating and evaporation: A new approach to the modeling of the processes. Physics of Fluids 1 July 2023; 35 (7): 073311. https://doi.org/10.1063/5.0158661
The final published version can be found at: https://doi.org/10.1063/5.0158661

Droplet Heating and Evaporation: A New Approach to the Modelling of the Processes

D.V. Antonov,[1] S. Tonini,[2] G.E. Cossali,[2] V.V. Dolgikh,[1] P.A. Strizhak,[1] and S.S. Sazhin*[3]

[1)] *Heat and Mass Transfer Laboratory, National Research Tomsk Polytechnic University, 30 Lenin Avenue, Tomsk 634050, Russian Federation*

[2)] *Department of Engineering and Applied Sciences, Università degli Studi di Bergamo, Viale Marconi 6, 24044 Dalmine (BG), Italy*

[3)] *Advanced Engineering Centre, School of Architecture, Technology and Engineering, University of Brighton, Brighton BN2 4GJ, United Kingdom.*

(*Electronic mail: S.Sazhin@brighton.ac.uk.)

A new model for mono-component droplet heating/evaporation is developed, tested, and applied to the analysis of in-house experimental data. The new model links the previously developed liquid phase model, using the analytical solution to the heat transfer equation at each timestep, and the gas phase model, using the solution to the equations of the conservation of mass, momentum and energy leading to an explicit expression for the Nusselt number and implicit expression for evaporation rate of the droplet. The latter expressions are used as boundary conditions for the liquid phase model. The new model is verified using a comparison between its predictions of the droplet temperatures and radii for very large liquid thermal conductivity (1000 W/(m·K) and those of the model, using the assumption that the thermal conductivity of liquid is infinitely large. The closeness between the predictions of these models supports the reliability of both. The model is validated using the experimental data obtained at the Heat Transfer laboratory of Tomsk Polytechnical University with regard to the heating/evaporation of droplets. The deviations between the measured and predicted droplet radii and temperatures in most cases are shown to be within experimental error margins.

I. INTRODUCTION

Interest in the problem of modelling droplet heating, evaporation and related problems has been stimulated by numerous engineering, pharmaceutical, and environmental applications[1–4]. Various approaches to this problem have been discussed in numerous papers summarised in monographs[3,5]. Commonly used approaches to modelling these processes use the assumptions that the thermal conductivity of liquid is infinitely large and heat and mass transfer in the gas phase can be described using the Abramzon and Sirignano model[6] (e.g.[7,8]). The first assumption is commonly based on the observation that the thermal conductivity of liquid is much larger than that of gas. This reasoning would be applicable to steady state processes, but the processes during droplet heating/evaporation are transient during which the processes in the liquid phase are controlled by thermal diffusivity rather than by thermal conductivity. The former is much larger for gas than for liquid[3].

The importance of finite liquid thermal conductivity in the analysis of droplet heating/evaporation was demonstrated in a number of models summarised in[3]. It seems that the most practically useful among these models is the one using the analytical solution to the heat transfer equation in the droplet based on the Robin boundary condition at its surface. This solution was implemented into numerical codes and used at each timestep of the calculations[9]. In the latter paper, a simplified version of the Abramzon and Sirignano model[6] was applied for modelling of the processes in the gas phase. The effect of recirculation inside the droplet due to its motion relative to the ambient gas was considered using the Effective Thermal Conductivity (ETC) model[3].

One of the most important assumptions of the Abramzon and Sirignano model[6] is that the density of the mixture of air and vapour above the surface of the evaporating droplet is constant (it does not depend on the distance from this surface). This assumption may become questionable for droplets evaporating in high temperature environments and a model that did not use it was developed in[10]. Although the latter model does not predict an explicit expression for the evaporation rate (as was the case with the Abramzon and Sirignano model[6]), finding this rate using the approach developed in[10] is much simpler than using a rigorous approach, based on the mass, momentum and energy conservation equations. This simplicity was based on keeping only the leading term in the asymptotic expansion of the vapour mass fraction equation. This approach was rigorously investigated and justified in[11]. The analysis of[10] used the assumption that there are no temperature gradients in the droplet (liquid thermal conductivity is infinitely large). This paper focuses on the development and testing of the new model incorporating the liquid phase model developed in[9] and gas phase model developed in[10]. The key ideas of these models and the details of incorporating the models into a numerical algorithm are described in Section II. In Section III the predictions of the numerical algorithm based on the new model are verified using a comparison of the predictions of this algorithm in the limit of infinitely large liquid thermal conductivity and the prediction of the algorithm based on the model described in[10]. The effect of various parameters on droplet heating and evaporation characteristics, predicted by the new model, are illustrated in Section IV. The results of validation of the predictions of the new model using in-house experimental data are presented in Section V. The key findings are summarised in Section VI.

II. MODEL AND NUMERICAL ALGORITHM

As mentioned in Section I, the model was built by combining the liquid phase model developed in[9] and the gas phase model developed in[10]. Basic ideas of the latter models are summarised in Appendices A and B. The model applies to single component droplets, and spherical symmetry is assumed. The heat transfer process in a liquid droplet with radius R_d is described using the analytical solution to the heat transfer equation for temperature T[3,9]:

$$\frac{\partial T}{\partial t} = \kappa \left(\frac{\partial^2 T}{\partial R^2} + \frac{2}{R} \frac{\partial T}{\partial R} \right), \tag{1}$$

where t is time, R is the distance from the droplet centre, κ is thermal diffusivity.

The liquid thermophysical properties are considered to be constant during each timestep. The droplet radius changes with time due to swelling and evaporation but is considered to be constant during each timestep. The analytical solution to Eq. (1), as presented in[3], is reproduced in Appendix A (Expression (7)). Boundary condition (4) was used, and the values of h (convective heat transfer coefficient) and R_d (droplet radius) were predicted by the gas phase model[10], which uses the analytical solutions to the quasi-steady species, momentum, and energy equations (see Appendix B, Eqs. (9)-(12)). The latter solutions were obtained assuming that thermal conductivity, heat capacity and the mass diffusion coefficient are uniform in the gas phase, while the dependence of the gas density on temperature is explicitly considered. The main outcome of these solutions is an implicit equation to evaluate the droplet evaporation rate (Eq. (19)), and the gas temperature distribution (Eq. (14)). The latter allows one to evaluate h.

The effect of the droplets' movement on their heating is introduced via the following corrections to Nu (cf. a similar correlation used in[6]):

$$\mathrm{Nu}_{\mathrm{mov}} = \mathrm{Nu} \left\{ \mathscr{F} \left(1 + \mathrm{Re} \cdot \mathrm{Pr}\right)^{1/3} \right\}, \tag{2}$$

where

$$\mathscr{F} = \max\left[1, \mathrm{Re}^{0.077}\right],$$

$\mathrm{Nu}_{\mathrm{mov}}$ is the moving droplet's Nusselt number, Nu is defined by Expression (20), Pr and Re are Prandtl and Reynolds numbers, respectively.

Similarly, the effect of the droplets' movement on their evaporation is introduced via the following corrections to $\hat{m}_{ev}$[3,6]:

$$\hat{m}_{ev,\mathrm{mov}} = \hat{m}_{ev} \left\{ \mathscr{F} \left(1 + \mathrm{Re} \cdot \mathrm{Sc}\right)^{1/3} \right\}, \tag{3}$$

where $\hat{m}_{ev,\mathrm{mov}}$ is the normalised evaporation rate for the moving droplets, $\hat{m}_{ev}$ is defined by Expression (19). There are other ways to consider the effect of convection on the heat and mass transfer between the droplet and the surrounding gas, like the approach based on film theory[12]. The present method is used here for its simplicity and straightforwardness.

The effects of thermal radiation and droplet support were considered assuming that both radiative heat and heat supplied by conduction from the support are homogeneously and instantaneously distributed throughout the whole droplet volume. The effective absorption factor was approximated by a power function of droplet radius (see[3,13] for the details). Both effects are relatively small for the cases to be considered.

The model was implemented in Matlab R2020a code and 100 terms were used in the series (7) (see Appendix A). Timesteps of 0.0001 s were used to calculate the heating/evaporation of droplets, and 10,000 cells along the droplet radius were used to calculate the integrals used in (7). The roots of Eq. (8) were obtained using the bisection method with an absolute error of not more than 10^{-12}.

This choice of parameters for use in calculations was based on the observation that further increase in the number of terms in the series and in the number of cells, and decrease in the timestep and errors in the bisection method do not affect the results of calculation.

The following key steps of the numerical algorithm were used:

1. The initial temperature distribution inside and outside the droplet is assumed or the distributions predicted at the previous timestep are used.
2. The droplet volume average temperature is calculated.
3. The values of liquid and effective thermal conductivity are calculated.
4. The other liquid properties at the average droplet temperature are calculated.
5. The thermophysical properties in the ambient gas (air)/vapour mixture at the reference temperature, are calculated using the '1/3 rule'[14].
6. The evaporation rate is calculated using Equation (3).
7. The values of the Nusselt number (Expression (2)) and the corresponding convective heat transfer coefficient h are calculated.
8. The temperature distribution inside and outside the droplet is calculated using the solutions for liquid and gas phases.
9. The droplet's radius at the end of the timestep, taking into account its evaporation and swelling, is calculated.
10. The calculations return to Step 1 and the process is repeated.

III. VERIFICATION OF THE NUMERICAL ALGORITHM

The verification of the numerical algorithm based on the new model was performed using a comparison of its predictions in the limiting case of a droplet with unrealistically large thermal conductivity (1000 W/(m·K) with the predictions of the original model[10], which assumes infinite thermal conductivity. The values of input parameters presented in Table I were used for calculations.

Results of the comparison between the time evolution of $(R_d/R_{d0})^2$ and T_d/T_{d0} predicted by the model presented in Section II with liquid thermal conductivity 1000 W/(m·K), and the model described in[10] are presented in Figure 1. As

TABLE I. The values of the parameters used for model verification.

Parameter	Value	Description
R_{d0}	10^{-5} m	Initial droplet radius
T_{d0}	300 K	Initial droplet temperature
T_a	600 K	Ambient temperature
p	101325 Pa	Ambient pressure
M_v	0.226446 kg/mole	Vapour molar mass
M_a	0.02895 kg/mole	Ambient air molar mass
T_{cr}	723 K	Critical temperature of n-hexadecane

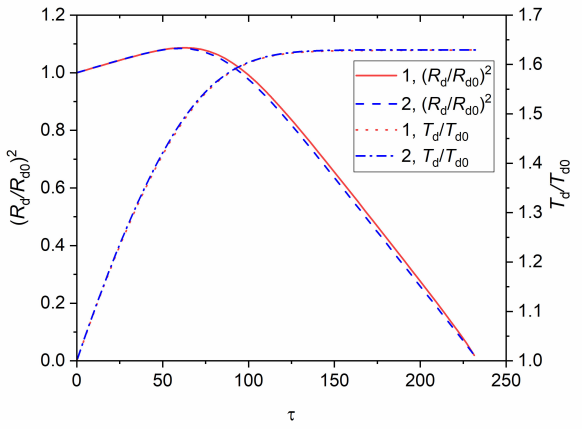

FIG. 1. Non-dimensional droplet radii squared $(R_d/R_{d0})^2$ and non-dimensional volume average temperature T_d/T_{d0} versus non-dimensional time $\tau = tD_{v0}/R_{d0}^2$, where D_{v0} is the vapour diffusion coefficient taken at the initial temperature T_{d0}, predicted by the model presented in Section II, with liquid thermal conductivity equal to 1000 W/(m·K) (curves "1") and the model described in[10] (curves "2"). Input parameters presented in Table I were used in calculations.

follows from this figure, the matching between the results predicted by both models is satisfactory (the difference between the predicted values of $(R_d/R_{d0})^2$ and T_d/T_{d0} is less than 1%). This gives us confidence in using the new algorithm for the analysis of droplet heating/evaporation.

IV. PARAMETRIC STUDY

The parametric study focuses on the investigation of the effect of finite liquid thermal conductivity on droplet heating/evaporation. At first the same input parameters as for the plots in Figure 1 were used. Two values of thermal conductivity of n-hexadecane were considered: 1000 W/(m·K) (to approximate the Infinite Thermal Conductivity model) and its realistic temperature dependence (see Table II in Appendix C). Plots of droplet radii versus time predicted for both cases are presented in Figure 2a. As follows from this figure, taking into account the effect of realistic liquid thermal conductivity leads to a 5.4% reduction in the droplet lifetime.

The same plots as in Figure 2a, but for $R_{d0} = 3$ mm and $T_g = 1200$ K, are presented in Figure 2b. As follows from that figure, in the case of the larger droplets, the effect of finite

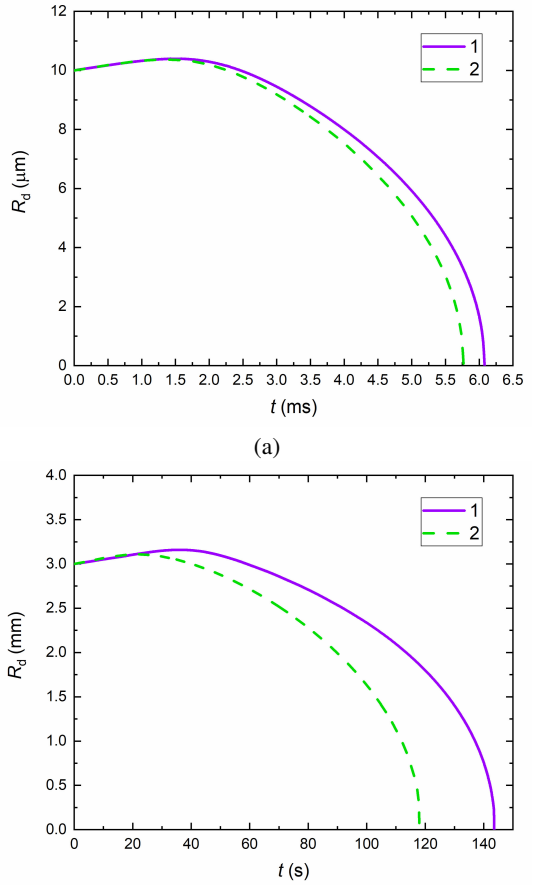

FIG. 2. Plots of droplet radii versus time predicted by the Infinite Thermal Conductivity (ITC) model (with a liquid thermal conductivity equal to 1000 W/(m·K) (curve "1") and a realistic temperature dependent thermal conductivity of n-hexadecane (see Table II in Appendix C) (curve "2") for the input parameters presented in Table I (a); the same as in Figure 2a but for $R_{d0} = 3$ mm and $T_g = 1200$ K (b).

liquid thermal conductivity leads to a 21.7% reduction in the droplet lifetime. This reduction is much larger than in the case shown in Figure 2a and should be considered in practical engineering applications.

Plots of normalised droplet temperature versus normalised distance from the droplet centre for five time instants for the same input parameters as in Figure 2a (considering the effect of finite liquid thermal conductivity) are presented in Figure 3. The presence of a temperature gradient in the droplet is clearly seen at the start of the heating process. At $t = 3$ ms, this gradient becomes close to zero throughout the droplet volume, which may justify the applicability of the ITC model in this case.

The same plots as in Figure 3, but for $R_{d0} = 3$ mm and $T_g = 1200$ K and different time instants, are shown in Figure 4. The reported results confirm that the effects of temperature gradient in the liquid phase are important at the beginning of the process, but less important at its final stages.

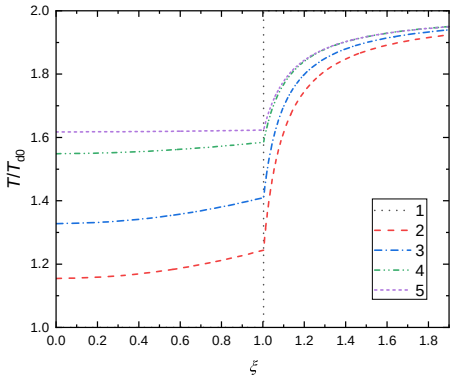

FIG. 3. Plots of normalised liquid and gas temperature versus normalised distance from the droplet centre $\xi = R/R_d$ for the input parameters presented in Table I and liquid n-hexadecane thermal conductivity given in Table II in Appendix C at $t = 0$ ms (curve "1"), $t = 0.5$ ms (curve "2"), $t = 1$ ms (curve "3"), $t = 2$ ms (curve "4"), and $t = 3$ ms (curve "5").

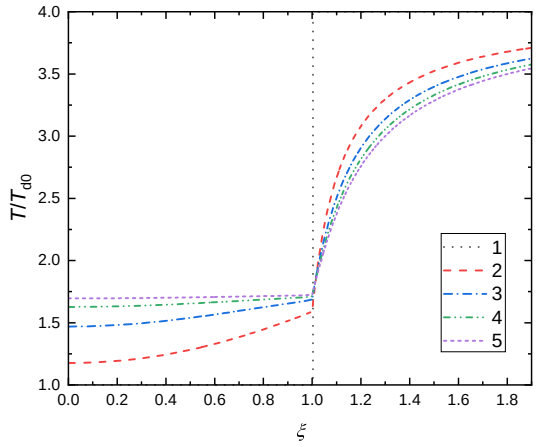

FIG. 4. Plots of normalised liquid and gas temperature versus $\xi = R/R_d$ for the input parameters presented in Table I but for $R_{d0} = 3$ mm and $T_g = 1200$ K at $t = 0$ s (curve "1"), $t = 20$ s (curve "2"), $t = 40$ s (curve "3"), $t = 60$ s (curve "4"), and $t = 80$ s (curve "5").

V. MODEL PREDICTIONS VERSUS EXPERIMENTAL DATA

This section focuses on the comparison of the predictions of the new model with experimental results obtained at the Heat and Mass Transfer Laboratory of the National Research Tomsk Polytechnic University. In the experiments, droplets were heated in a Nabertherm R 50/250/13 tubular muffle furnace (temperature range 300 K to 3000 K). Suspended n-decane droplets were introduced into the registration area using a motorized manipulator, at the end of which there was a solder of a low-inertial type K thermocouple with a diameter of 0.2 mm.

Figure 5 shows a schematic, and an actual image, of a droplet on a thermocouple holder. The thermocouple junction was located at the centre of the droplet, and, according to

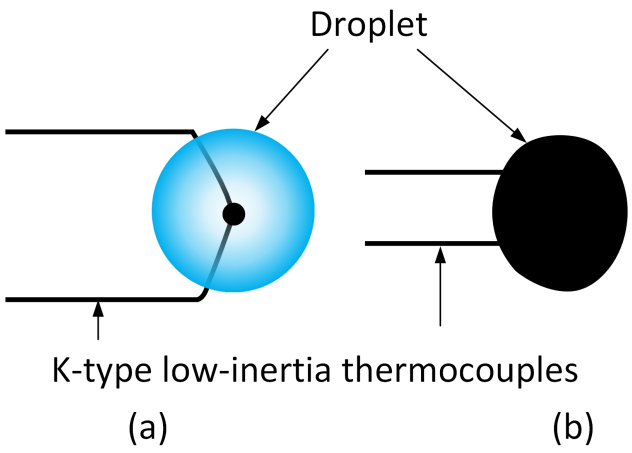

FIG. 5. A schematic (a) and actual image (b) of a droplet mounted on a low-inertia type K thermocouple holder of diameter 0.2 mm.

video frame analysis, the maximum displacement of that junction from the centre did not exceed 20%. These displacements contributed to random measurement errors.

The n-decane droplets were generated using an electronic Finnpipette Novus dispenser with fluid intake functions 5 to 50 μl (with a step of 0.1 μl). The initial diameter of the n-decane droplets in the three series of experiments was 0.85 ± 0.05 mm, 0.95 ± 0.05 mm, and 1.05 ± 0.05 mm, respectively. Five to ten experiments were performed for each case. Gas temperature in the furnace (T_a) and average droplet temperature (T_d) were measured using a National Instruments data acquisition complex and K-type low-inertia thermocouples. Systematic errors of temperature measurements based on the manufacturer's specification were ± 3 K, while systematic errors of time registration were ± 0.1 s. The initial droplet temperature was monitored by a thermocouple and was in the range $298 - 318$ K. The ambient atmospheric pressure was assumed to be equal to 101325 Pa. Gas temperature was monitored using a thermocouple and maintained at the level of 760 ± 10 K.

The registration area was illuminated using a MultiLed QT projector (GS Vitec GmbH, Germany) to improve the image contrast of the droplets. The droplet evaporation process was recorded using a high-speed Phantom Miro M310 video camera. The images were recorded with a frequency of 1000 fps, resolution of 512×512 pixel, and exposure time of 1 μs. Video recording started when droplets reached the registration area. Air velocity relative to the droplet was 0.2 ± 0.05 m/s. It was measured by a Testo 425 thermal anemometer. The time required for the droplet to reach the registration area (2.5 s) was considered in the analysis of recorded dependence of droplet radii on time. The video frames were processed using specially developed MatLab code. The systematic errors of measured droplet initial radii were less than ± 0.044 mm (± 2 pixels). The total errors (sum of systematic and random errors) of the measurements were less than ± 0.05 mm (see Ref.[15] for more details).

An example of video images of an evaporating droplet sup-

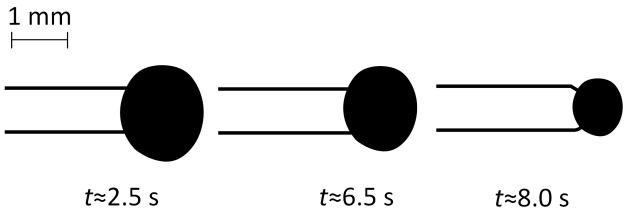

FIG. 6. An example of video images of an evaporating droplet supported by a thermocouple for $T_g = 760 \pm 10$ K, $T_0 = 300 \pm 10$ K and $R_{d0} = 0.85 \pm 0.05$ mm.

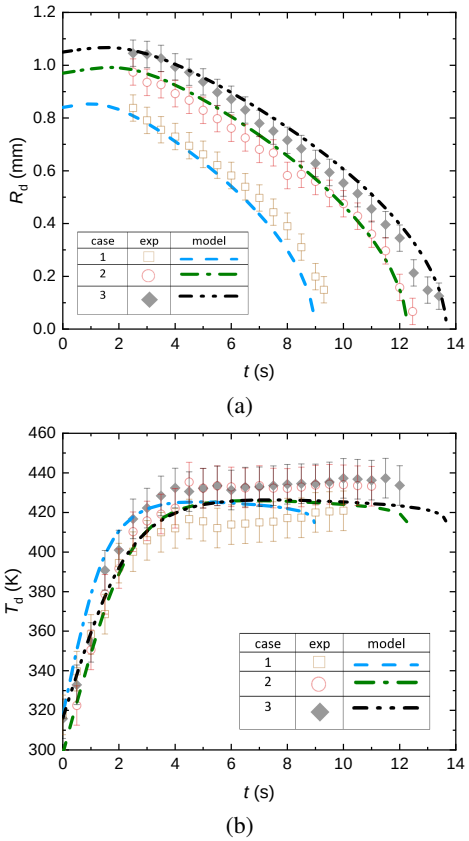

FIG. 7. Experimental and modelling results for time evolution of radii (a) and average temperature (b) of n-decane droplets for $T_g = 760 \pm 10$ K and $T_0 = 300 \pm 10$ K and $R_{d0} = 0.85 \pm 0.05$ mm (1), $R_{d0} = 0.95 \pm 0.05$ mm (2), and $R_{d0} = 1.05 \pm 0.05$ mm (3).

ported by a thermocouple at three time instants is presented in Figure 6.

The predicted and observed values of R_d and T_d versus time for heated and evaporated n-decane droplets are compared in Figure 7. Three initial values of droplet radii and temperatures were used. Gas temperature was 760 K. As can be seen from this figure, modelling results agree with observations within experimental error margins in most cases. The deviation between the predicted and observed results at the final stage of droplet evaporation (up to 7% and 10% for droplet radii and temperatures, respectively) is linked to several limitations of

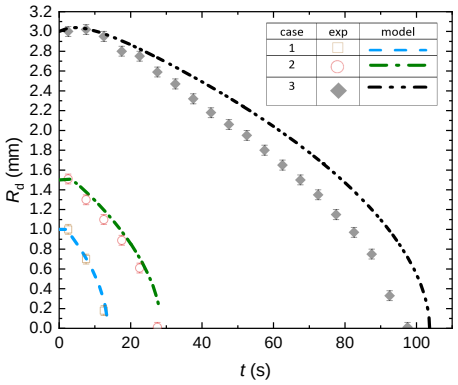

FIG. 8. Experimental and modelling results for time evolution of radii of n-decane droplets for $T_g = 760 \pm 10$ K and $T_0 = 300 \pm 10$ K and $R_{d0} = 1.0 \pm 0.05$ mm (1), $R_{d0} = 1.5 \pm 0.05$ mm (2), and $R_{d0} = 3.0 \pm 0.05$ mm (3).

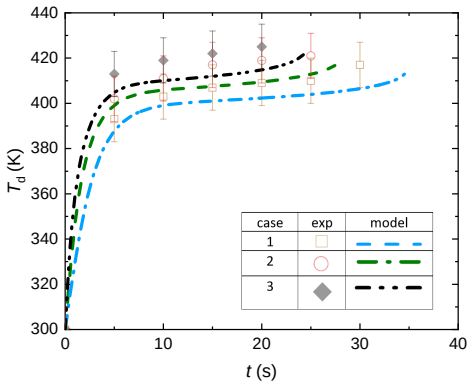

FIG. 9. Experimental and modelling results for time evolution of average temperatures of n-decane droplets for $R_{d0} = 1.5 \pm 0.05$ mm, $T_0 = 300 \pm 10$ K, and $T_g = 700 \pm 10$ K (1), $T_g = 900 \pm 10$ K (2), $T_g = 1100 \pm 10$ K (3).

the model used in the analysis. These include the assumptions that droplets are spherical and that the effects of the droplet support are small[13].

The same images as shown in Figure 7a but for initial droplet radii in the range 1 to 3 mm are presented in Figure 8. As follows from this figure, when droplet radii are increased from 1 to 3 mm the agreement between the experimental and modelling results is poorer. For droplets with initial radii 1 mm, the observed and predicted times required for complete evaporation differ by no more than 1.5%, while for droplets with initial radii 3 mm, they differ by up to 6%. This is related to the fact that large droplets tend to become non-spherical. In such cases, use of the model described in this paper to model them is less reliable.

The same images as shown in Figure 7b but for initial droplet radii 1.5 ± 0.05 mm and gas temperatures in the range 700 K to 1100 K are shown in Figure 9. As follows from Figure 9, in all cases, the deviation between experimental data and predictions of the model does not exceed the errors of experimental measurements, although the observed average

droplet temperatures tend to be higher than the predicted ones.

VI. CONCLUSIONS

A new model for mono-component droplet heating and evaporation was developed, tested, and applied to the analysis of experimental data. The main idea of the new model lies in linking the previously developed liquid phase model described in[9] and gas phase model described in[10]. The liquid phase model uses the analytical solution to the heat transfer equation in a spherically symmetric droplet with the Robin boundary condition at its surface. This analytical solution is incorporated into the numerical code and applied at each timestep of the calculations. The gas phase model uses the solution to the equations of the conservation of mass, momentum and energy leading to the explicit expression for the Nusselt number and implicit expression for droplet evaporation rate. The latter expressions were used as boundary conditions for the liquid phase model.

The effects of liquid motion inside the droplet were considered using the Effective Thermal Conductivity (ETC) model. The corrections to the convective heat transfer coefficient and evaporation rate due to droplet movement were taken into account using Correlations (2) and (3). The effect of droplet support was considered using the model developed in[13], based on the assumption that heat supplied from a droplet support is instantaneously and homogeneously distributed throughout the droplet volume.

The new model was verified using a comparison between its predictions of the droplet radii and temperatures for very large liquid thermal conductivity (1000 W/(m·K) and those of the model described in[10], using the assumption that liquid thermal conductivity is infinitely large. The closeness between both predictions (the deviation was less than 1%) supports the reliability of both models.

The experimental and modelling results referring to time evolution of radii and average temperatures of n-decane droplets for gas temperature $T_g = 760$ K and initial droplet temperatures and radii in the ranges $298 - 318$ K and $0.84 - 1.05$ mm, respectively, were shown to be close (the deviation between them was within experimental error margins). The deviation between the observed and predicted results at the final stage of droplet evaporation can be attributed to several limitations of the model used in the analysis. These include the assumptions that droplets are spherical and the effects of the droplet support are small.

It was shown that when droplet radii increased from 1 to 3 mm the agreement between experimental and modelled results becomes less convincing. This is related to the observation that large droplets tend to be non-spherical, and in such cases the reliability of the model described in this paper is questionable. It was shown that the maximal deviation between experimentally observed average droplet temperatures and predictions of the model is comparable with the errors of experimental measurements for gas temperatures in the range 700 to 1100 K. The observed average droplet temperatures, however, tended to be higher than the predicted ones.

APPENDICES

A. Liquid phase model

Assuming that the processes are spherically symmetric, the heat transfer in the droplet is described using the Eq. (1).

The model uses the solution to Equation (1) ($R \le R_d$) with the Robin boundary condition at the droplet surface:

$$k_l \left.\frac{\partial T}{\partial R}\right|_{R=R_d-0} = h(T_{\text{eff}} - T_s), \tag{4}$$

$$T_{\text{eff}} = T_g + \frac{\rho_l L \dot{R}_d}{h}, \tag{5}$$

where T_g ambient gas temperature, $\dot{R}_d = \mathrm{d}R_d/\mathrm{d}t$, L the specific heat of evaporation, h the constant convection heat transfer coefficient, and the initial condition

$$T(t=0) = T_{d0}(R). \tag{6}$$

$T = T(R,t)$ is assumed to be a twice continuously differentiable function at $R \le R_d$.

The solution to (1) in this case is presented as[3]:

$$T(R,t) = \frac{R_d}{R} \sum_{n=1}^{\infty} \left\{ q_n \exp\left[-\kappa_R \lambda_n^2 t\right] \right.$$

$$- \frac{\sin\lambda_n}{\| \nu_n \|^2 \lambda_n^2} \mu_0(0) \exp\left[-\kappa_R \lambda_n^2 t\right] - \frac{\sin\lambda_n}{\| \nu_n \|^2 \lambda_n^2}$$

$$\left. \times \int_0^t \frac{\mathrm{d}\mu_0(\tau)}{\mathrm{d}\tau} \exp\left\{-\kappa_R \lambda_n^2 \left[t-\tau\right]\right\} \mathrm{d}\tau \right\}$$

$$\times \sin\left\{ \lambda_n \left(\frac{R}{R_d} \right) \right\} + T_g(t), \tag{7}$$

λ_n are solutions to the following equation:

$$h_0 \sin\lambda + \lambda \cos\lambda = 0, \tag{8}$$

$$h_0 = \frac{h R_d}{k_l)} - 1,$$

$$\tilde{T}_0(R) = \frac{R T_{d0}(R)}{R_d},$$

$$q_n = R_d^{-1} \| \nu_n \|^{-2} \int_0^{R_d} \tilde{T}_0(R) \sin\left[\lambda_n \left(\frac{R}{R_d} \right) \right] \mathrm{d}R,$$

$$\| \nu_n \|^2 = \frac{1}{2} \left(1 + \frac{h_0}{h_0^2 + \lambda_n^2} \right) = \frac{1}{2} \left(1 - \frac{\sin 2\lambda_n}{2\lambda_n} \right),$$

$$\kappa_R = \frac{k_l}{c_l \rho_l R_d^2},$$

$$\mu_0(t) = \frac{h T_g(t) R_d}{k_l},$$

ρ_l, k_l, and c_l are the liquid density, thermal conductivity, and specific heat capacity, respectively.

The solution to Eq. (8) leads to a set of positive eigenvalues λ_n ($n = 1, 2, ...$) numbered in ascending order. The values of h and $\dot{R}_d$ are inferred from the gas phase model (see Appendix B).

B. Gas phase model

Following[5,10], the investigation of the processes in the gas phase surrounding a droplet uses the steady-state mass, momentum and energy balance equations for the vapour and gas (air) mixture:

$$\frac{\mathrm{d}}{\mathrm{d}R}\left\{R^2 \rho_v U - R^2 D_v \rho_{\text{total}} \frac{\mathrm{d}Y_v}{\mathrm{d}R}\right\} = 0, \tag{9}$$

$$\frac{\mathrm{d}}{\mathrm{d}R}\left\{R^2 \rho_a U - R^2 D_v \rho_{\text{total}} \frac{\mathrm{d}Y_a}{\mathrm{d}R}\right\} = 0, \tag{10}$$

$$\rho_{\text{total}} U \frac{\mathrm{d}U}{\mathrm{d}R} = \frac{\mathrm{d}p_{\text{total}}}{\mathrm{d}R} + \mu_{\text{mix}}\left\{\frac{\mathrm{d}^2 U}{\mathrm{d}R^2} + \frac{2}{R}\frac{\mathrm{d}U}{\mathrm{d}R}\right\}, \tag{11}$$

$$\rho_{\text{total}} U c_{p,\text{mix}} \frac{\mathrm{d}T}{\mathrm{d}R} = k_{\text{mix}}\left\{\frac{\mathrm{d}^2 T}{\mathrm{d}R^2} + \frac{2}{R}\frac{\mathrm{d}T}{\mathrm{d}R}\right\}, \tag{12}$$

where U is the Stefan flow velocity[3] and $R \geq R_d$ is the distance from the droplet centre. Thermophysical properties refer to the mixture of vapour (v) and air (a). They are assumed to be uniform, with the exception of the density. An extension of the model considering the dependence on temperature of all the thermophysical properties was presented in[16]). ρ_{total} and T depend on R. Partial (p_v and p_a) and total (p_{total}) pressures are inferred from the Dalton and ideal gas laws.

Equations (9)-(12) were solved using the following boundary conditions:

$$T(R=\infty) = T_{a,\infty}, \quad T(R=R_d) = T_s,$$

$$p_v(R=R_d) = p_{vs}(T_s), \quad Y_v(R=\infty) = Y_{v,\infty}.$$

The following equation for the conservation of mass follows from (9)-(10):

$$\rho_{\text{total}} U = \frac{|\dot{m}_{ev}|}{4\pi R^2}, \tag{13}$$

where $\dot{m}_{ev}$ is the droplet evaporation rate.

Eq. (13) allows us to decouple (12) from the other equations. The solution to (12) can be presented as:

$$T = (1 - A_{\text{TC}}(R))\, T_s + T_{a,\infty} A_{\text{TC}}(R), \tag{14}$$

where

$$A_{\text{TC}}(R) = \frac{\exp\left(-\frac{\hat{m}_{ev} R_d}{\text{Le} R}\right) - \exp\left(-\frac{\hat{m}_{ev}}{\text{Le}}\right)}{1 - \exp\left(-\frac{\hat{m}_{ev}}{\text{Le}}\right)}, \tag{15}$$

$\hat{m}_{ev} = |\dot{m}_{ev}|/(4\pi R_d D_v \rho_{a,\infty})$
Le $= k_{\text{mix}}/(D_v \rho_{a,\infty} c_{p,\text{mix}})$.
New variables

$$G = \ln(Y_a) = \ln(1 - Y_v), \quad \zeta = R_d/R, \quad \tilde{T} = T/T_{a,\infty}$$

lead to the following equation for G:

$$-G_{\zeta\zeta} + G_\zeta \frac{G_\zeta \theta e^G \tilde{T} + \left(1 + \theta e^G\right)\tilde{T}_\zeta + \varepsilon 2\zeta^3 G_\zeta^2}{\left[\left(1 + \theta e^G\right)\tilde{T} - \varepsilon \zeta^4 G_\zeta^2\right]}$$

$$= \varepsilon \frac{\zeta^2 G_\zeta^2 (\zeta^2 G_{\zeta\zeta\zeta} + 4\zeta G_{\zeta\zeta} + 2G_\zeta)}{\left[\varepsilon \zeta^4 G_\zeta^2 - \left(1 + \theta e^G\right)\tilde{T}\right]\frac{\hat{m}_{ev}}{\text{Sc}}} \tag{16}$$

where

$$\hat{m}_{ev} = -\frac{\mathrm{d}G}{\mathrm{d}\zeta}\tilde{\rho}, \tag{17}$$

$$\varepsilon = \frac{M_v D_v^2}{R_u T_{a,\infty} R_d^2}. \tag{18}$$

$\theta = (M_v - M_a)/M_a$, M_a and M_v are the molar masses of ambient gas and vapour, respectively, $\tilde{\rho} = \rho_{\text{total}}(R)/\rho_{\text{total}}(R=\infty)$, Sc is the Schmidt number.

The assumption that $\varepsilon = 0$ (its validity was justified in[11]) leads to the following equation for $\hat{m}_{ev}$:

$$\hat{m}_{ev} + \left(\frac{\hat{m}_{ev}}{1 - \exp\left(-\frac{\hat{m}_{ev}}{\text{Le}}\right)} - \text{Le}\right)\left(\tilde{T}_s - 1\right) = \mathscr{G}, \tag{19}$$

where

$$\mathscr{G} = -\hat{p}_{v,\text{cr}} \ln\left\{\frac{\hat{p}_{v,\text{cr}} - \hat{p}_{vs}}{\hat{p}_{v,\text{cr}} - Y_{v\infty}}\right\},$$

$$\hat{p}_{vs} = \frac{p_{vs} M_v}{R_u T_{a\infty} \rho_{a\infty}}, \quad \hat{p}_{v,\text{cr}} = 1 + \theta(1 - Y_{v\infty}),$$

R_u the universal gas constant, $p_{vs}(T_s)$ the saturation vapour pressure.

h was inferred from the Nusselt number Nu. Following[10], for stationary droplets the latter was estimated as:

$$\text{Nu} = 2\left(\frac{\hat{m}_{ev}}{\text{Le}} \frac{\exp\left(-\frac{\hat{m}_{ev}}{\text{Le}}\right)}{1 - \exp\left(-\frac{\hat{m}_{ev}}{\text{Le}}\right)}\right). \tag{20}$$

The temperature gradient at the droplet surface is calculated from Expression (14). Nu predicted by Expression (20) is close to 2 when $\hat{m}_{ev}$ is small (the Stefan flow can be ignored).

TABLE II. The approximations of transport and thermodynamic properties of n-hexadecane: subscript *l* shows the liquid phase, while subscript *v* shows the vapour phase.

Parameter	Approximation	Unit
p_{sat}[19]	$\exp\left(156.06-\frac{15015}{T_s}-18.941\cdot\log_{10}(T_s)+681.72\cdot T_s^2\right)$	Pa
D_v[20]	$\frac{1.975T_{\text{ref}}^{1.75}}{92902P_{\text{gas}}}$	m^2/s
k_l[21]	$0.189-1.2226\cdot10^{-4}\cdot T-1.3059\cdot10^{-7}\cdot T^2$	W/(m· K)
c_l[19]	$\frac{370.35+0.23147\cdot T+0.00068632\cdot T^2}{M_v}$	kJ/(kg·K)
ρ_l[19]	$\frac{268.07M_v}{0.25287^{1+\left(1-\frac{T}{723}\right)^{0.31143}}}$	kg/m^3
L[19]	$10.156\cdot10^4\cdot(1-(T_s/T_{\text{cr}}))^{0.45726}\cdot M_v^{-1}$	J/kg

TABLE III. The approximations of transport and thermodynamic properties of n-decane: subscript *l* shows the liquid phase, while subscript *v* shows the vapour phase.

Parameter	Approximation	Unit
p_{sat}[22]	$133.322\times10^{26.512-\frac{3358.4}{T_s}-6.1174\cdot\log(T_s)-3.3225\cdot10^{-10}\cdot T_s+4.8554\cdot10^{-7}\cdot T_s^2}$	Pa
D_v[21]	$\left(-0.03116+1.707510^{-4}\cdot T_{\text{ref}}+3.793\cdot10^{-7}\cdot T_{\text{ref}}^2\right)\cdot10^{-4}$	m^2/s
k_v[21]	$-1.13\cdot10^{-3}+8.1090\cdot10^{-6}\cdot T+9.6092\cdot10^{-8}\cdot T^2$	W/(m· K)
c_{pv}[22]	$\left(31.78+0.74489\cdot T-1.0945\cdot10^{-4}\cdot T^2-2.267\cdot10^{-7}\cdot T^3+9.3458\cdot10^{-11}\cdot T^4\right)/M_v$	J/(kg·K)
k_l[21]	$0.186-1.183\cdot10^{-4}\cdot T-1.9797\cdot10^{-7}\cdot T^2$	W/(m· K)
c_l[22]	$\frac{79.741+1.6926\cdot T-4.5287\cdot10^{-3}\cdot T^2+4.9769\cdot10^{-6}\cdot T^3}{M_v}$	kJ/(kg·K)
ρ_l[22]	$232.8\cdot0.2524^{-\left(1-\frac{T}{T_{\text{cr}}}\right)^{0.2857}}$	kg/m^3
L[22]	$71428\cdot\left(1-(T_s/T_{\text{cr}})\right)^{0.451}\cdot M_v^{-1}$	J/kg

C. Thermophysical properties

Tables II and III show the correlation used to calculate the thermophysical properties of n-hexadecane and n-decane, respectively. The gas mixture thermal conductivity is calculated according to the Wassiljewa relation[17]:

$$k_{mix}=\frac{k_a x_a}{x_a+A_{av}x_v}+\frac{k_v x_v}{x_v+A_{va}x_a} \tag{21}$$

where the coefficients A_{av} and A_{va} are obtained from the Lindsay and Bromley relationship[18] and k_a is calculated as in Table IV. The gas mixture specific heat capacity is calculated as mass averaged specific heat capacity of vapour and air, where the specific heat capacity of air c_{pa} is calculated using the formulae shown in Table IV.

TABLE IV. Thermal conductivity and specific heat capacity of air.

Parameter	Approximation	Unit
k_a[21]	$1.024\cdot10^{-2}-8.21\cdot10^{-6}\cdot T+1.41\cdot10^{-7}\cdot T^2-4.51\cdot10^{-11}\cdot T^3$	W/(m· K)
c_{pa}[22]	$\frac{29.643-5.1373\cdot10^{-3}\cdot T+1.3106\cdot10^{-5}\cdot T^2-4.8325\cdot10^{-9}\cdot T^3}{M_a}$	J/(kg·K)

ACKNOWLEDGMENTS

Research was supported by the Russian Science Foundation (Grant No. 23-69-10006, https://rscf.ru/project/23-69-10006/).

[1] H. Erbil, Advances in Colloid and Interface Science **170**, 67–86 (2012).
[2] B. Sobac, T. Talbot, B. Haut, A. Rednikov, and P. Colinet, Journal of Colloid and Interface Science **438**, 306–317 (2015).
[3] S. Sazhin, *Droplets and Sprays: Simple Models of Complex Processes* (Springer, 2022).
[4] Y. Wang, D. Alvares, H. Wan, R. Pizarro, and F. Shu, Phys. Fluids **35**, 063317 (2023).
[5] G. Cossali and S. Tonini, *Drop Heating and Evaporation: Analytical Solutions in Curvilinear Coordinate Systems* (Springer, 2021).
[6] B. Abramzon and W. Sirignano, International Journal of Heat and Mass Transfer **32**, 1605 (1989).
[7] A. Offner and J. Vanneste, Phys. Fluids **34**, 053320 (2022).
[8] N. Sen, Phys. Fluids **33**, 033311 (2021).

[9]S. Sazhin, P. Krutitskii, W. Abdelghaffar, E. Sazhina, S. Mikhalovsky, S. Meikle, and M. Heikal, International Journal of Heat and Mass Transfer **47**, 3327 (2004).
[10]S. Tonini and G. Cossali, International Journal of Thermal Science **57**, 45 (2012).
[11]S. Tonini, G. Cossali, E. Shchepakina, V. Sobolev, and S. Sazhin, Physics of Fluids **34**, 073312 (2022).
[12]S. Tonini and G. Cossali, International Journal of Thermal Science **75**, 194 (2014).
[13]P. Strizhak, R. Volkov, G. Castanet, F. Lemoine, O. Rybdylova, and S. Sazhin, International Journal of Heat and Mass Transfer **127**, 92–106 (2018).
[14]M. Yuen and L. Chen, Combust. Sci. Tech. **14**, 147–154 (1976).
[15]D. Antonov, P. Strizhak, R. Fedorenko, Z. Nissar, and S. Sazhin, Fuel **289**, 119814 (2021).
[16]G. Cossali and S. Tonini, International Journal of Heat and Mass Transfer **138**, 1166–1177 (2019).
[17]A. Wassiljewa, Physikalische Zeitschrift **5 (22)**, 737–742 (1904).
[18]A. Lindsay and L. Bromley, Ind. Eng. Chem. **42**, 1508–1511 (1950).
[19]R. Perry, D. Green, and J. Maloney, *Perry's Chemical Engineers'* (Platinum Edition, 1999).
[20]E. Fuller, P. Schetter, and J. Giddings, Ind. Eng. Chem. **58 (5)**, 18–27 (1966).
[21]C. Yaws, *Transport Properties of Chemicals and Hydrocarbons* (Gulf Professional Publishing, 2015).
[22]C. Yaws, *The Yaws Handbook of physical properties for hydrocarbons and chemicals* (Gulf Professional Publishing, 2015).